



Dynamic-based model for calculating the boulder impact force in debris flow

Chaoping YANG, Shaojie ZHANG, Yueping YIN, Hongjuan YANG, Fangqiang WEI

View online: <https://doi.org/10.1007/s11629-023-8441-7>

Articles you may be interested in

[Dynamic impact of boulders on different types of concrete dam](#)

Journal of Mountain Science. 2022, 19(10): 2920 <https://doi.org/10.1007/s11629-022-7419-1>

[Impact failure models and application condition of trees in debris-flow hazard mitigation](#)

Journal of Mountain Science. 2021, 18(7): 1874 <https://doi.org/10.1007/s11629-020-6510-8>

[Dynamic response analysis of blocks-combined dam under impact load](#)

Journal of Mountain Science. 2020, 17(11): 2827 <https://doi.org/10.1007/s11629-019-5619-0>

[Debris flow impact on flexible barrier: effects of debris-barrier stiffness and flow aspect ratio](#)


Journal of Mountain Science. 2019, 16(7): 1629 <https://doi.org/10.1007/s11629-018-5314-6>



[A 3-D DDA damage analysis of brick masonry buildings under the impact of boulders in mountainous areas](#)

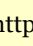

Journal of Mountain Science. 2018, 15(3): 657 <https://doi.org/10.1007/s11629-017-4453-5>


Original Article


Dynamic-based model for calculating the boulder impact force in debris flow

YANG Chaoping^{1,2}  <https://orcid.org/0009-0006-5205-2592>; e-mail: yang-chaoping@hotmail.com

ZHANG Shaojie^{1*}  <https://orcid.org/0000-0001-5908-9554>;  e-mail: sj-zhang@imde.ac.cn

YIN Yueping^{3*}  <https://orcid.org/0000-0001-5396-3933>;  e-mail: yyueping@mail.cgs.gov.cn

YANG Hongjuan¹  <https://orcid.org/0000-0003-0635-6764>; e-mail: yanghj@imde.ac.cn

WEI Fangqiang^{4,5}  <https://orcid.org/0000-0001-8734-0881>; e-mail: fqwei@cigit.ac.cn

*Corresponding author

¹ State Key Laboratory of Mountain Hazards and Engineering Resilience, Institute of Mountain Hazards and Environment, Chinese Academy of Sciences, Chengdu 610299, China

² University of Chinese Academy of Sciences, Beijing 100049, China

³ China Institute of Geological Environment Monitoring, Beijing 100081, China

⁴ Chongqing Institute of Green and Intelligent Technology, Chinese Academy of Sciences, Chongqing 400714, China

⁵ Chongqing School, University of Chinese Academy of Sciences, Chongqing 400714, China

Citation: Yang CP, Zhang SJ, Yin YP, et al. (2024) Dynamic-based model for calculating the boulder impact force in debris flow. Journal of Mountain Science 21(6). <https://doi.org/10.1007/s11629-023-8441-7>

© Science Press, Institute of Mountain Hazards and Environment, CAS and Springer-Verlag GmbH Germany, part of Springer Nature 2024

Abstract: The boulder impact force in debris flow is generally calculated by static methods such as the cantilever beam models. However, these methods cannot describe the dynamic scenario of boulder collision on structures, so the inertia and damping effects of the structures are not involved causing an overestimation on the boulder impact force. In order to address this issue, a dynamic-based model for calculating the boulder impact force of a debris flow was proposed in this study, and the dynamic characteristics of a cantilever beam with multiple degrees of freedom under boulder collision were investigated. By using the drop-weight method to simulate boulders within debris flow, seven experiments of drop-weight impacting the cantilever beam were used to calibrate the error of the dynamic-based model. Results indicate that the dynamic-based model is able to reconstruct the impact force history on the cantilever beam during impact time and the error of dynamic-based model is 15.3% in calculating boulder impact force, significantly outperforming the

cantilever beam model's error of 285%. Therefore, the dynamic-based model can overcome the drawbacks of the static-based models and provide a more reliable theoretical foundation for the engineering design of debris flow control structures.

Keywords: Debris flow; Impact force; Boulder collision; Dynamic-based model; Engineering design

Notation

F	= Boulder impact force within debris flow (KN)
V	= Impact velocity (m/s)
\hat{k}	= Effective contact stiffness (N/m)
c_d	= Additional mass coefficient (-)
m_f	= Mass of the slurry interacting with boulder (kg)
T	= Duration of the boulder impact force (s)
S	= Distance of the boulder motion (m)
R	= Boulder radius (m)
K_c	= Empirical load reduction factor (-)
c	= Experimental regression coefficients (-)
ρ_s	= Density of the solid particle (kg/m ³)
W	= Weight of the boulder (KN)
L	= Length of the cantilever beam (m)
γ	= Kinetic energy reduction coefficient (-)

Received: 28-Oct-2023

Revised: 15-Feb-2024

Accepted: 15-Apr-2024

C_1 = Elastic deformation coefficients of the boulder (-)
C_2 = Elastic deformation coefficients of the structure (-)
α = Angle of the boulder impacting structure (°)
M = Mass matrix (kg)
C = Damping matrix (N·m/s)
K = Stiffness matrix (N/m)
u = Deflection of the cantilever beam (m)
ε = Strains measured by FBG ($\mu\varepsilon$)
g = Corresponding Green function (-)
Δt = Sampling interval (s)
m = Number of sampling points (-)
K_ε = Strain sensitivity coefficient of FBG (nm/ $\mu\varepsilon$)
K_T = Temperature sensitivity coefficient of FBG (nm/°C)
$\Delta\varepsilon$ = Strain variations measured by FBG ($\mu\varepsilon$)
ΔT = Temperature variations (°C)
$\Delta\lambda$ = Central wavelength offset (nm)
l = Length of the cantilever beam (m)
x = Distance between the measuring point and the fixed end of cantilever beam (m)
h = Height of the cross section of the cantilever beam (m)
h_f = Heights of the hammer (m)
λ_0 = Initial central wavelength of FBG (nm)
E = Elasticity modulus (MPa)
ρ = Density (kg/m ³)

1 Introduction

Debris flows can cause damage downstream through erosion, deposition, and impact; among these processes, the damage caused by the impact force of debris flow is the most significant, as it frequently contributes to the failure of debris flow control

structures (Hu et al. 2011; Liu et al. 2019; Vagnon 2020; Zhang et al. 2019a). Debris flow constitutes a two-phase fluid comprising slurry and solid particles. The impact force of debris flow can generally be divided into slurry dynamic pressure and boulder impact force (Iverson 1997; Song et al. 2019; Zhang 1993; Zhang and Chen 2017), with the latter being several times—or sometimes more than 10 times—the former and is the primary cause of structure failure (Ng et al. 2018; Zeng et al. 2015). Therefore, it is important to accurately calculate the boulder impact force of a debris flow to support the engineering design of debris flow control structures (Shen et al. 2018; Wang et al. 2023). Current models for determining the boulder impact force of a debris flow are listed in Table 1 and can be divided into rigid modes (Haehnel and Daly 2004; Paczkowski et al. 2012) and non-rigid modes (He et al. 2016; Huang et al. 2007; Hungr et al. 1984; Kwan et al. 2019; Luo et al. 2022; Si et al. 2022; Zhou et al. 2020). Rigid modes, such as the impulse conservation method (Engineers, 2000), functional principal method (Consolazio 2009), and contact stiffness method (Haehnel and Daly 2004) assume that the boulders within debris flow as well as the structures are rigid. However, the impact force of debris flow can cause structure deformation, and the assumption of a rigid mode is not consistent with the actual collision situation and usually overestimates the boulder impact force of the debris flow (Huang et al. 2022; Stolle et al. 2018). Therefore, if the stiffness of a structure is not significantly greater than that of the boulders, its deformation should be considered (Stolle et al. 2018). Structure deformation caused by boulder collision is considered in non-rigid models (Table 1), which are divided into two types depending on the structure deformation characteristics. One is represented by the local damage to a structure due to boulder collision (Majeed et al. 2019). The Hertz Contact Theory Model (He et al. 2016; Huang et al. 2007; Kwan et al. 2019; Mizuyama 1979) is commonly used to describe this impact scenario and calculate the boulder impact force of a debris flow, with the structure assumed to be stationary and flat without bending deformation during impact. Boulders within debris flow are assumed to be spheres moving at a certain speed, and the collision between the boulders and a

Table 1 Impact force calculation model.

Calculation models		Equations	Sources
Rigid modes		$F = V\sqrt{\hat{k}(M + c_d m_f)}$	Haehnel and Daly 2004
		$F = \frac{\pi MV}{2T}$	Paczkowski et al. 2012
		$F = \frac{MV^2}{S}$	Sayed and Attia 2012
Non-rigid modes	Hertz contact theory model	$F = 30800V^{1.2}R^2g$	Huang et al. 2007
		$F = 48200V^{1.2}R^2g$	Mizuyama 1979
		$F = 50000V^{1.2}R^2g$	Yamaguchi 1985
		$F = 4000K_cV^{1.2}R^2$	Kwan et al. 2019
		$F = c\left(\frac{n+1}{3c}\pi R^3V^2\rho_s\right)^{\frac{n}{n+1}}$	He et al. 2016
Cantilever beam model		$F = \sqrt{\frac{3EIV^2W}{gL^3}}$	Zhang 1993
		$F = \sqrt{MV^2k}$	Hungr et al. 1984
		$F = 0.0105\varepsilon_{max} - 2.6507$	Zhang and Chen 2017
	$F = \gamma V \sin\alpha \sqrt{\frac{W}{C_1 + C_2}}$	Zhou et al. 2020	

structure satisfies the Hertz contact conditions (Hertz 1882). Engineering structures in the field, such as bridge piers and comb-tooth dams, are appropriately simplified as cantilever beams according to their boundary conditions (Wang et al. 2016). This can yield bending deformation when impacted by debris flow (Zhang et al. 2019b). The other type of impact force calculation is based on the bending deformation theory of the cantilever beam (Hung et al. 1984; Yong et al. 2020; Zhang 1993; Zhang and Chen 2017; Zhou et al. 2020).

A debris flow control structure, which can be simplified as a cantilever beam, will not only be bent but also forced to vibrate by the impact force of a debris flow, which is typically a dynamic process. Therefore, besides the peak value of the impact force of the debris flow, it is crucial to consider also the dynamic response of the cantilever beam to the boulder impact force during impact force determination (Marchelli and De Biagi 2019). The dynamic process of boulder collision on structures is neglected by the calculation models listed in Table 1, indicating that almost all investigations focusing on determining the boulder impact force are static-based (Eu et al. 2019; Zhang et al. 2007). Although static-based methods for calculating the boulder impact force are simple, they do not consider the damping and inertial effects of the cantilever beam in the vibration process, resulting in overestimations (Huang and Zhang 2022). Recently, after simplifying the cantilever beam as a single-degree-of-freedom (SDOF) structure (Fig. 1a), Tang and Hu (2018) used the dynamic equation of a SDOF structure to describe the vibration process of the cantilever beam due to the impact of the debris flow and derived an equation for the impact force of the debris flow. According to I SDOF structure assumption, all the mass of the cantilever beam is concentrated on a mass point, which is then connected to the fixed end

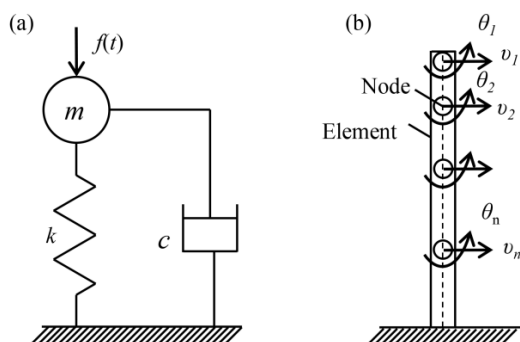


Fig. 1 (a) Single-degree-of-freedom (SDOF) and (b) multi-degree-of-freedom (MDOF) structures.

by a spring and damper; hence, only one generalized coordinate is needed to determine the motion position of this mass point. However, as shown in Fig. 1b, this assumption ignores the fact that the cantilever is a multi-degree-of-freedom (MDOF) structure, resulting in low calculation accuracy of the impact force of the debris flow (Chen et al. 2019; Clough and Penzien 1993).

To improve the calculation accuracy of the boulder impact force of a debris flow, the dynamic process induced by boulder collision is described by the MDOF motion differential equation, which is solved using the modal coordinate transformation and Duhamel integral. A dynamic-based model for calculating the boulder impact force of a debris flow is established and verified by drop-weight impact tests.

2 Methodology

2.1 Dynamic-based model for calculating the boulder impact force

The dynamic process of the cantilever beam induced by the collision of the boulders within debris flow can be described by the MDOF motion differential equation. Generally, the boulder impact force can be expressed as a function of the stiffness, damping, and mass of the cantilever beam (Clough and Penzien 1993).

$$M\ddot{u}(x, t) + C\dot{u}(x, t) + Ku(x, t) = F(t) \quad (1)$$

where, $M\ddot{u}(x, t)$, $C\dot{u}(x, t)$, and $F(t)$ represent the inertial force vector (N), damping force vector (N), elastic force vector (N), and boulder impact force vector (N), respectively. After solving Eq. (1), we obtain a solution depicting the relationship between the strain of the cantilever beam and the boulder impact force.

$$\varepsilon = \frac{3h(l-x)}{x^2(3l-x)} \sum_{i=1}^n \frac{\phi_i \phi_i^T}{M_i \omega_{id}} \int_0^t F_i(\tau) e^{-\xi_i \omega_i(t-\tau)} \sin \omega_{id}(t-\tau) d\tau \quad (2)$$

More details on Eq. (2) are given in Appendix 1. For simplicity, Eq. (2) is abbreviated as follows:

$$\varepsilon(t) = \int_0^t g(t-\tau) f(\tau) d\tau \quad (3)$$

where $\varepsilon(t)$ is the time history of the bending strain caused by the boulder impact force and $g(t)$ is the corresponding Green's function, namely the i -th node strain response under the impulse load. where $f(t)$ is the time history of the boulder impact force.

Assuming that the continuous action time of the impact force on the cantilever beam is $[0, T]$, Δt is the sampling interval, m is the number of sampling points,

and f_i is the boulder impact force at time t ($t = i\Delta t$). Eq. (3) is discretized and converted into a system of linear equations, which can be expressed in matrix form as follows:

$$\begin{Bmatrix} \varepsilon_1 \\ \varepsilon_2 \\ \vdots \\ \varepsilon_m \end{Bmatrix} = \begin{bmatrix} g_1 & & & \\ g_2 & g_1 & & \\ \vdots & \vdots & \ddots & \\ g_m & g_{m-1} & \dots & g_1 \end{bmatrix} \begin{Bmatrix} f_0 \\ f_1 \\ \vdots \\ f_{m-1} \end{Bmatrix} \Delta t \quad (4)$$

Eq. (4) is a mathematical formula for calculating the impact force of boulders within debris flow, which was established based on the motion differential equation of a MDOF cantilever beam. Therefore, Eq. (4) is applicable to engineering bodies that can be simplified as cantilever beams, such as bridge piers and comb-tooth dams. To use Eq. (4) to calculate the boulder impact force, its input parameters, including the strain time history data and Green's function, should be determined first.

2.2 Experiments of boulder impacts on cantilever beam

A measurement system for the boulder impact force must be conceived to verify the precision of the dynamic-based model. In the measurement system, a cantilever beam is used as the object impacted by boulders. The input parameter of the model is the continuous bending strain along the cantilever beam; therefore, multiple measurement points along the axial direction of the cantilever beam are required to capture the deformation characteristics of the MDOF cantilever beam. Fiber Bragg grating (FBG) sensors can accommodate distributed measurements and can simultaneously sense the bending strain at multiple measurement points using wavelength-division multiplexing (Braunfelds et al. 2021). Therefore, FBG sensors were selected as sensing cells in the measurement system of the boulder impact force.

2.2.1 Measurement system based on FBG sensors

As shown in Fig. 2, the FBG sensor-based measurement system comprises mainly a boulder impact simulation subsystem, cantilevered measuring device, and data acquisition component.

The boulder impact simulation subsystem contains a drop hammer with a weight of 10 kg and a pulley. The amplitude of the impact force induced by the collision of the drop hammer on a reinforced

concrete beam is approximately equivalent to that of the boulder impact force of a natural debris flow (Zhang and Chen 2017). Therefore, the drop hammer represents a boulder within debris flow, which is raised to different heights by the pulley and then released to collide with the reinforced concrete beam to simulate diverse boulder impact effects.

The cantilever measuring device comprises primarily four FBG sensors, a piezoelectric sensor, and a reinforced concrete cantilever beam. The central wavelength of the FBG sensors can be shifted owing to variations in temperature and strain; therefore, the central wavelength of the FBG sensors is dependent on temperature and strain, and the relationship is as follows (Zhang et al. 2019b):

$$\Delta\lambda = K_\varepsilon \Delta\varepsilon + K_T \Delta T \quad (5)$$

where K_ε is the strain sensitivity coefficient of the FBG sensors (nm/ $\mu\varepsilon$), K_T is the temperature sensitivity coefficient of the FBG sensors (nm/ $^\circ\text{C}$), $\Delta\varepsilon$ and ΔT denote the strain and temperature variations, respectively, and $\Delta\lambda$ represents the central wavelength offset. All experiments were performed under indoor conditions and constant room temperature, with $\Delta\lambda$ being dependent only on the strain.

As shown in Fig. 3a, 3b, the FBG sensors were welded to a steel bar, which was polished in advance

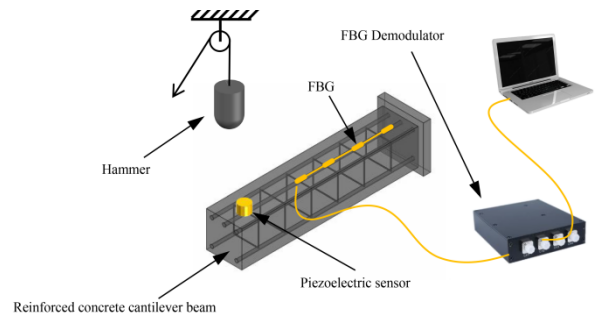


Fig. 2 Measurement system based on FBG sensors.

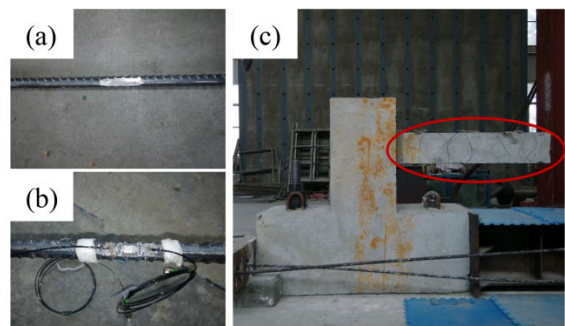


Fig. 3 Cantilever sensing device. (a) Installation of the FBG sensors on the steel bar; and (b) Diagram of field experimental device.

for easier installation. The steel bar and FBG sensors were buried in the tensile area of the concrete cantilever beam for protection.

Four FBG sensors (i.e. four measurement points, namely #A, #B, #C, and #D) were fixed on the steel bar along its axial direction; their related parameters are listed in Table 2, where h_f is the distance between the measuring point and the fixed end of the reinforced concrete cantilever beam (cm) and λ_0 is the initial central wavelength of each sensor (nm). A piezoelectric sensor was used to quantify the impact force of the hammer. Prior to its deployment, the sensor was calibrated using the dynamometre standards outlined in JJG144-92. The detailed parameters of the sensor are listed in Table 3.

In Fig. 3c, the cantilever sensing device is highlighted with a red circle; its geometric size was 0.2 m × 0.2 m × 1.0 m. The physical parameters of the reinforced concrete cantilever beam are listed in Table 4. The T-shaped beam was rigidly fixed to the ground with bolts, and its stiffness was much greater than that of the cantilever sensing device. Therefore, the sensing device could be regarded as a cantilever beam capable of elastic deformation.

In Table 4, E and ρ are the elastic modulus (MPa) and density (kg/m³), respectively, which can be determined in accordance with the Concrete Structural Design Code GB50010-2010.

The data acquisition system comprised an FBG demodulator and a computer. The FBG demodulator is the most crucial component; its performance parameters, i.e. wavelength range, wavelength resolution, accuracy, and sampling frequency, are 1,528–1,568 nm, 0.1 × 10⁻¹² nm, ±0.5 × 10⁻¹² nm, and 100 Hz, respectively.

2.2.2 Test conditions

To verify the accuracy of the dynamic-based model for calculating the boulder impact force of a debris flow, a series of impact tests were performed, during which the drop hammer collided with the cantilever sensing device. The impact height of the drop hammer was considered as an independent variable and was varied systematically to investigate its effect on the calculated boulder impact force. For this purpose, we used the pulley to lift the drop hammer to six different heights, i.e. 0.2, 0.4, 0.6, 1.0, 2.0, and 7.0 m, from the upper surface of the reinforced concrete cantilever beam; the corresponding impact velocities of the hammer were 1.98, 2.8, 3.43, 4.43, 6.26, and 11.71 m/s. Once the

height was set, the drop hammer was dropped freely to impact the cantilever sensing device. The distance between the impact point and the fixed end of the cantilever sensing device was 90 cm, and the central wavelength change of each FBG sensor was recorded during each test.

Table 2 FBG sensor parameters.

FBG sensor	h_f (cm)	K_e (nm/ $\mu\epsilon$)	λ_0 (nm)
A	5	0.001382071	1,553.642
B	20	0.001374983	1,549.632
C	40	0.001378464	1,545.533
D	60	0.001367618	1,537.254

Table 3 Piezoelectric sensor parameters.

Upper capacity (KN)	h_f (cm)	Resolution ratio (N)	Error (%)
10	90	0.3052	3

Table 4 Physical parameters of the reinforced concrete cantilever beam.

Parameter	Concrete	Longitudinal bar	Stirrup
E (MPa)	3.0 × 10 ⁴	2.0 × 10 ⁵	2.1 × 10 ⁵
ρ (kg/m ³)	2,360	7,850	7,850

3 Results

When the drop hammer collided with the cantilever sensing device, tensile bending strain was induced in the steel bar within the tensile region of the cantilever sensing device, causing a shift in the central wavelengths of the FBG sensors affixed to the steel bar. The offset of the central wavelengths was subsequently modulated using the FBG demodulator and collected using a data acquisition system. Finally, the optical signal of each FBG sensor was transformed into the bending strain of the corresponding measurement point using Eq. (5).

As shown in Fig. 4, the dynamic process of the bending strain at measurement point #A indicates that as the impact height of the drop hammer increases, the FBG sensor at point #A records a gradual increase of the bending strain value, corresponding to an increase of the impact force on the cantilever beam. Using the test condition with a 20-cm impacting height as an example, the bending strain at point #A exhibits a sudden increase upon impact of the drop hammer on the cantilever beam, followed by a rapid decrease to zero after reaching its maximum value. Subsequently, this value oscillates around zero because of the free vibration of the cantilever sensing device and

eventually returns to its initial strain value as the energy dissipates. The bending strain at point #A can be fully restored to its initial value under the test conditions of 0.2, 0.4, 0.6, 1.0 m, and 2.0 m, indicating the elastic behavior of the sensing device. However, under a test condition of 7 m, the strain at point #A exhibits residual deformation owing to the irreversible plastic deformation of the steel bar within the sensing device. As the height of the drop weight increases, the plastic deformation of the steel bar within the cantilever sensing device increases accordingly. However, this study adopted a dynamics-model model to calculate the boulder impact force of a debris flow that is suitable for linear elastic systems. Therefore, to ensure the validity of the results and minimize non-linear influences, such as plastic deformation, the height of the drop weight was limited to below 7 m.

3.1 Impact time determination

The impact force is a dynamic load exhibiting time history. Determining the precise duration of its action is essential. Before the drop hammer acts on the cantilevered sensing device, the strain within the device remains at zero. However, once impacted by the drop hammer, the device generates a forced vibration that demonstrates an initial surge increase, followed by a subsequent dramatic bending strain decrease. As the impact subsides, the cantilever beam undergoes free vibration and gradually returns to its original state owing to its inherent elasticity, damping mechanism, and inertial forces. In summary, the impact behavior caused by the drop hammer acting on the device can be divided into three stages: no vibration prior to impact, forced vibration during impact, and free vibration after impact. The duration of the impact force effect lies

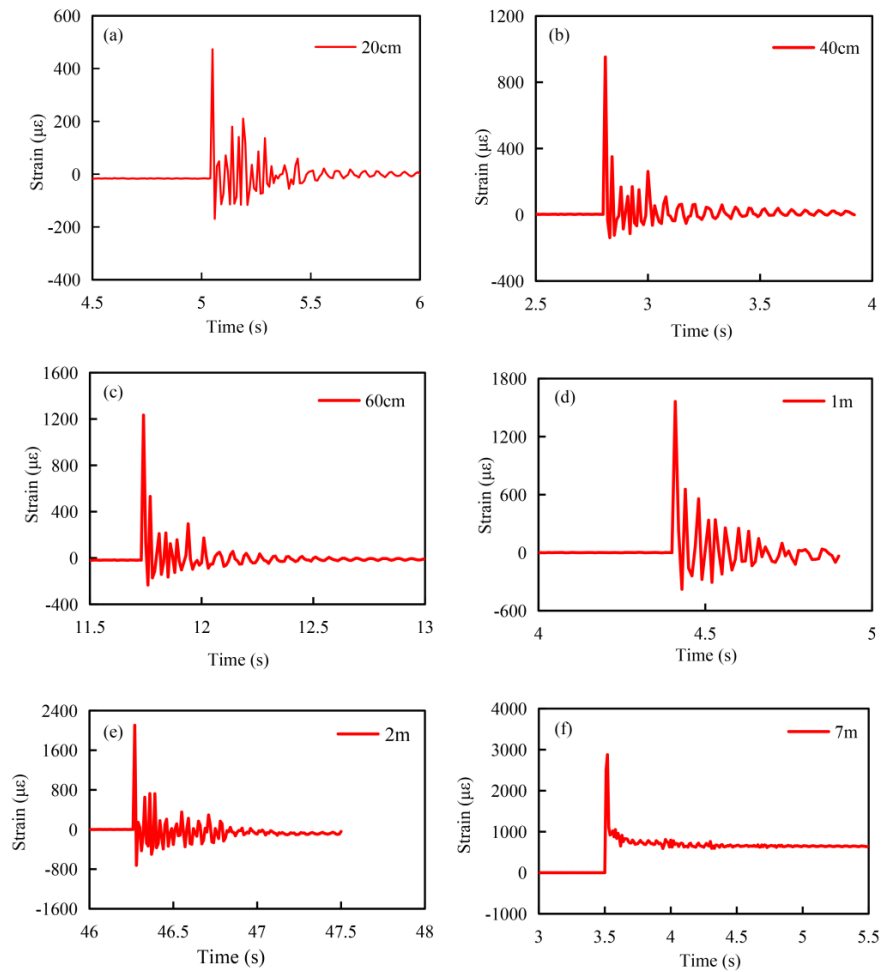


Fig. 4 Strain of the tested beam at measurement point #A under different impact heights.

solely within the second stage. The temporal length can be determined by measuring the triangular base length. As illustrated in Fig. 5, the duration of the impact force is 0.02 s across all test conditions.

3.2 Calculation of the boulder impact force using the dynamic-based model

Before using Eq. 4 to calculate the boulder impact force of the debris flow, it is necessary to obtain the strain and Green's function of the cantilever sensing device. The bending strains measured using FBG sensor #A during the impact process are listed in Table 5. There are three methods for determining Green's function: theoretical analysis, experimental analysis, and numerical analysis (Chen et al. 2019; Mao et al. 2010; Zhang et al. 2019c). In this study, Green's function was acquired using theoretical analysis. Green's function can be formulated as follows:

$$G(t) = \frac{3h(l-x)}{x^2(3l-x)} \sum_{l=1}^n \frac{\phi_l \phi_l^T}{M_l \omega_l} e^{-\xi_l \omega_l t} \sin \omega_l t \quad (6)$$

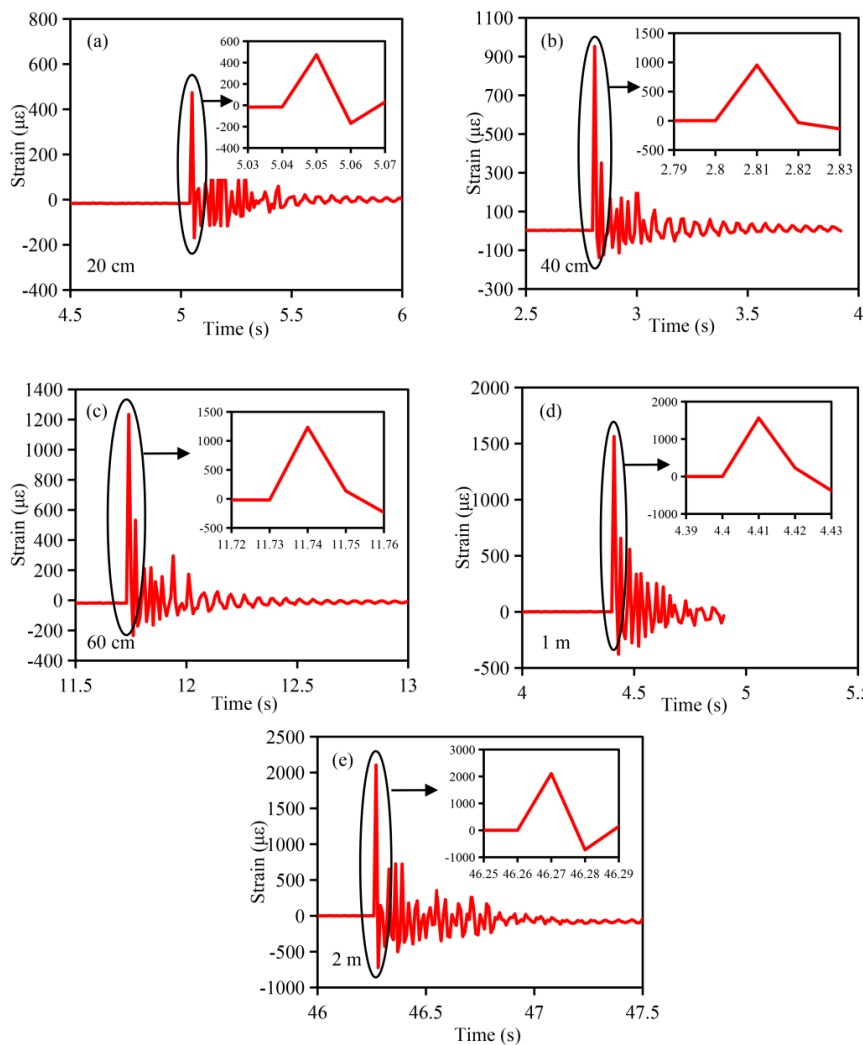


Fig. 5 Determination of the duration of the impact force under different impact heights.

Table 5 Strain data and corresponding impact times.

Test conditions	Time (s)	Strain (µε)	Test conditions	Time (s)	Strain (µε)
1	5.04	0.00	4	4.40	0.00
	5.05	473.13		4.41	1,562.77
	5.06	-169.02		4.42	228.46
2	2.80	0.00	5	46.26	0.00
	2.81	952.27		46.27	2,103.20
	2.82	-30.68		46.28	-722.10
3	11.73	0.00			
	11.74	1,233.49			
	11.75	136.85			

where M_i is the generalised mass of the cantilever sensing device, ω_i is the i -th natural frequency of the device, ξ_i is the i -th damping ratio, and Φ_i is the i -th vibration mode. Using the finite element method in the Dynamics of Structures (Clough and Penzien 1993), the cantilever sensing device can be discretised into a 14-degrees-of-freedom cantilever beam based on the

locations of both the FBG sensors and the drop weight, as depicted in Fig. 6. Green's function between point #A and the action point of the impact force is rewritten as Eq. 7, after neglecting the damping effect.

$$G(t) = \frac{3h(l-x)}{x^2(3l-x)} \sum_{i=1}^{14} \frac{\phi_i \phi_i^T}{M_i \omega_i} \sin \omega_i t \tag{7}$$

Based on Eq. (7), the corresponding Green's function at time t ($t = i\Delta t$) can be determined and the Green's function matrix can be assembled. Subsequently, the strains in Table 5 are substituted into Eq. (4) to calculate the boulder impact force of the debris flow, as shown in Fig. 7.

The boulder impact force in Fig. 7 first increases and then decreases during the collision of the drop hammer with the cantilever sensing device, which is consistent with the time history change law of the bending strain. The peak value of the impact time history increases significantly owing to the increase in the falling height of the drop hammer, indicating that the impact force increases as the impact height of the drop hammer increases.

3.3 Verification on the dynamic-based model

To verify the error of the dynamic-based model in calculating the boulder impact

force within a debris flow, a piezoelectric sensor was installed at the impact point of the cantilever sensing device to measure the impact force of the drop hammer. The sampling frequency of the FBG demodulator was set to 1,000 Hz, and a drop-weight impact test was conducted at a height of 10 cm. The impact force of the drop hammer was calculated using Eq. (4). The

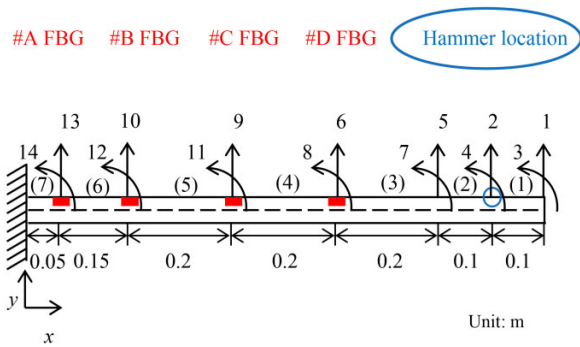


Fig. 6 Finite Element Discretization of the measuring device into a 14-Degrees-of-Freedom structure (7 translational degrees of freedom and 7 rotational degrees of freedom). The blue circle represents the hammer location, while the red rectangle indicates the positions of FBG sensors.

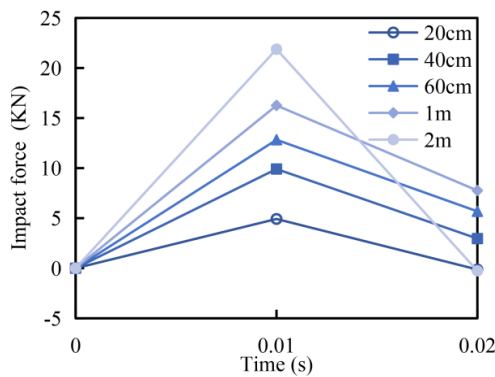


Fig. 7 Boulder impact force of a debris flow calculated using Eq. (4) under different impact heights.

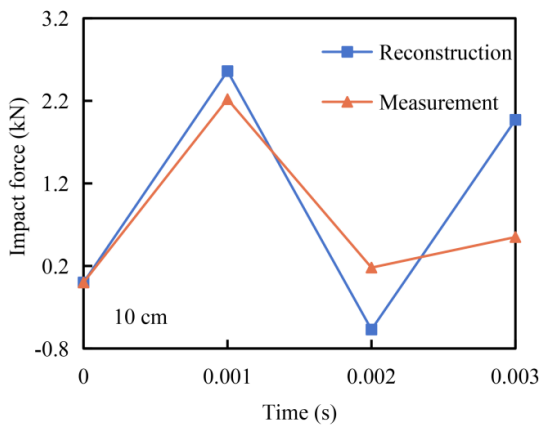


Fig. 8 Impact force derived from tests and the dynamic-based model under the impact height of 10 cm.

calculated and measured impact forces of the drop hammer are shown in Fig. 8.

As shown in Fig. 8, the peak impact force measured by the piezoelectric sensor was 2.22 KN, whereas the value calculated using the dynamic-based model was 2.56 KN. Consequently, the systematic

error in calculating the impact force of the stones using the proposed theoretical relationship was approximately 15.3%. One reason for the calculation error of the dynamic-based model is that the damping effect was not considered in the calculation of Green's function, causing overestimation. Another reason is the performance of the FBG demodulator used in the tests. The duration of the impact force of the drop hammer acting on the cantilever sensing device was very short, posing a challenge to the FBG demodulator due to its sampling frequency, which was only 100 Hz. Consequently, some key peak data may have been missed, resulting in lower measurements.

4 Discussion

4.1 Comparison with static-based models

As shown in Table 5, five tests of the drop hammer impacting the cantilever sensing device from different falling heights were performed. Currently, three static-based methods, namely the material mechanics method (Zhang, 1993), energy method (Hung et al. 1984), and Chen Guangxi's formula (Zhou et al. 2020), have been developed to determine the boulder impact force of a debris flow by calculating the bending strain of a cantilever beam. The impact force acting on the cantilever induced by the drop hammer in each impact test was calculated using the three static-based methods as well as the introduced dynamic-based method. All four impact force calculations are shown in Fig. 9, where the advantage of the dynamic-based method in calculating the boulder impact force of a debris flow becomes clear.

The pink curve derived using the dynamic-based method is lower than the other three curves derived using the static-based methods. Therefore, the impact force calculated using the static-based methods is greater than that calculated by the dynamic-based method; in particular, the impact forces from the material mechanics method and energy method are approximately 3–5 times greater than that of the dynamic-based method. For the engineering design of debris flow control and disaster prevention structures in China, the material mechanics method is commonly used to calculate the boulder impact force of a debris flow. However, engineering applications demonstrate that the material mechanics method usually overestimates the impact force (Lu et al. 2019), and the

comparative results of this study confirm this conclusion, as two of the static-based methods assume that the impact energy of the drop hammer is converted to bending strain energy of the cantilever beam. However, the falling height of the drop hammer continuously increases, and the impact force acting on the cantilever beam can be increased. As the impact force causes the cantilever beam to yield, indentations occur on the surface of the cantilever beam, which means that not all the impact energy of the drop hammer is converted into elastic strain energy of the cantilever beam, and part is absorbed by the grooves in the form of plastic strain energy. The principle of Chen Guangxi's formula is consistent with the energy method; however, the kinetic energy reduction coefficient, which is obtained from experiments, is introduced on the basis of the energy method, and the peak impact force calculation result is 1.2–2.0 times higher than that of the dynamic-based model. The kinetic energy reduction coefficient has a significant effect on the calculation results of this method.

4.2 Result differences between the static-based models and dynamic-based model

As shown in Fig. 9, the boulder impact forces calculated using the static-based models were significantly greater than that obtained using the dynamic-based model. This discrepancy is consistent with the results of other studies (Chen et al. 2017; Lu et al. 2019). For example, Zhou (1991) employed a static-based model to calculate the impact force of debris flow incidents in the Jiangjia Ravine. They predicted the impact force by conducting on-site surveys. They found that the static-based calculations consistently overestimated the impact force. This difference can be attributed to the assumption of the static approach that all boulder impact energy is converted entirely into bending deformation energy of the cantilever beam. In fact, an investigation of debris flow gullies revealed that impact indentations may be generated during the impact of boulders on structures (Fig. 10). This means that the elastic–plastic strain energy of the structures partially consumes the boulder impact energy. The energy conversion process of a boulder impact structure is expressed by Eq. (8) according to the energy conservation law (Kennedy 1976):

$$KE_B = SE_S + E_P + KE_S \quad (8)$$

where KE_B , SE_S , E_P , and KE_S represent the stone-

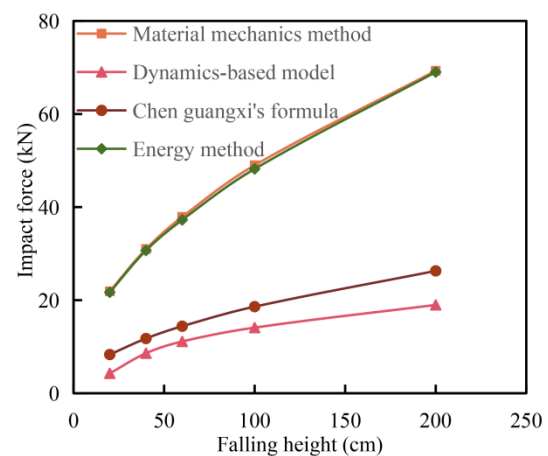


Fig. 9 Boulder impact force of a debris flow calculated using various methods.



Fig. 10 Impact indentations generated on structures in Li County.

impact kinetic energy, structural bending strain energy, structural elastic–plastic strain energy, and kinetic energy of the structure, respectively. Eq (8) indicates that once indentations are generated by debris flow boulders on the surface of the structure, the boulder impact energy is transformed into bending strain energy, elastic–plastic strain energy, and kinetic energy of the structure, and the elastic–plastic model is suitable for describing this impact case. However, if no indentations are formed, the boulder impact energy is converted into bending strain energy and kinetic energy of the structure; in this case, the interaction between the boulders and the cantilever beam should be classified as an elastic collision. No indentations were observed on the surface of the cantilever beam in the five impact tests listed in Table 5. Therefore, the impact energy of the drop hammer in this study was converted into bending strain energy and kinetic energy of the cantilever beam. Subsequently, the kinetic energy ultimately dissipates through damping

and inertia effects, which can be mathematically described by Eq. (1). Static-based methods assume that all impact energy is converted into bending strain energy of the cantilever beam, regardless of the inertial and damping effects of the cantilever beam; therefore, the calculated impact force is overestimated.

5 Conclusions

The interaction between boulders within debris flow and a cantilever beam is essentially a dynamic process. Traditional static-based methods cannot describe this dynamic scenario or consider the damping and inertial effects of the structure, causing an overestimation of the boulder impact force. To address this issue, the MDOF motion differential equation was used to describe the collision process between debris flow boulders and a cantilever beam, and a dynamic-based model for calculating the boulder impact force was proposed. The conclusions are as follows:

(1) Considering the damping and inertial effects of the cantilever beam, the error of the dynamic-based model related to the boulder impact force was calibrated using an FBG-sensor-based measuring system, and was found to be 15.3%, i.e. much lower than those of static-based methods.

(2) When applying the dynamic-based model in engineering practice, a prerequisite must be satisfied. The dynamic-based model is derived by solving the MDOF motion differential equation, which calculate the debris flow impact force induced by boulder collision on the cantilever beam; thus, it can only be applied to engineering structures that share similar characteristics with cantilever beams, such as comb-tooth dams and bridge piers. Such engineering structures are susceptible to bending deformation when subjected to boulder impact. Conventionally, the dynamic parameters of debris flow, such as the velocity and mass of the boulders, are important factors for calculating the boulder impact force, which can be

estimated based on the local geological and topographical conditions and the material dimensions of the structures. Using these parameters as input conditions, the boulder impact force that the structures endure can be determined. However, the necessary input parameters of the dynamic-based model are the bending strain and corresponding Green's functions, which are obtained through indoor tests and are different from those of conventional methods. Hence, further investigations based on the dynamic-based model should be performed in relation to engineering practice.

Acknowledgments

This work was supported by the National Natural Science Foundation of China (U2244227), National Key R&D Program of China (2023YFC3007205), and National Natural Science Foundation of China (No. 42271013).

Author Contribution

YANG Chaoping: Writing-original draft, Data curation. ZHANG Shaojie: Writing-original draft Supervision, Review, Funding acquisition. YIN Yueping: Funding acquisition, Supervision. YANG Hongjuan: Experiment, Data curation. WEI Fangqiang: Supervision.

Ethics Declaration

Availability of Data/Materials: Data is available on reasonable request from the corresponding author.

Conflict of Interest: The authors declare that they have no known competing financial interests or personal relationships that could have appeared to influence the work reported in this paper.

Electronic Supplementary Material

Supplementary materials (Appendix 1) are available in the online version of this article at <https://doi.org/10.1007/s11629-023-8441-7>

References

- Braunfelds J, Senkans U, Skels P, et al. (2021) FBG-based sensing for structural health monitoring of road infrastructure. *J Sens* 2021: 1-11. <https://doi.org/10.1155/2021/8850368>
- Chen HC, Zhang XR, Garcia BD, et al. (2019) Drop impact onto a cantilever beam: Behavior of the lamella and force measurement. *Interfacial Phenom Heat Transf* 7(1): 85-96. <https://doi.org/10.1615/InterfacPhenomHeatTransfer.2019.30975>
- Chen J, Wang Q, Chen Y, et al. (2017) Amending calculation on impact force of boulders in debris flow based on Hertz theory. *J Harbin Inst Technol* 49(02): 124-129. (In Chinese) <https://doi.org/10.11918/j.issn.0367-6234.2017.02.020>
- Clough RW, Penzien J (1993) *Dynamics of Structures*. 2nd ed. New York: McGraw-Hill.
- Consolazio GR (2009) *A Static Analysis Method for Barge-Impact Design of Bridges with Consideration of Dynamic*

- Amplification: Final Report, November 2009. University of Florida Dept of Civil and Coastal Engineering.
- Engineers American Society of Civil Engineers (2000) Minimum design loads for buildings and other structures. American Society of Civil Engineers.
- Eu S, Im S and Kim D (2019) Development of debris flow impact force models based on flume experiments for design criteria of soil erosion control dam. *Adv Civ Eng* 2019: 1-8. <https://doi.org/10.1155/2019/3567374>
- Haehnel RB, Daly SF (2004) Maximum Impact Force of Woody Debris on Floodplain Structures. *J Hydraul Eng* 130(2): 112-120. [https://doi.org/10.1061/\(ASCE\)0733-9429\(2004\)130:2\(112\)](https://doi.org/10.1061/(ASCE)0733-9429(2004)130:2(112))
- He SM, Liu W and Li XP (2016) Prediction of impact force of debris flows based on distribution and size of particles. *Environ Earth Sci* 75(4): 1-8. <https://doi.org/10.1007/s12665-015-5180-2>
- Hertz H (1882) Über die bruchung fester elastischer körper. *J Reine Angew Math* 92: 156-171. <https://doi.org/10.1515/crll.1882.92.156>
- Hu KH, Wei FQ, Li Y (2011) Real-time measurement and preliminary analysis of debris-flow impact force at Jiangjia Ravine, China. *Earth Surf Proc Land* 36(9): 1268-1278. <https://doi.org/10.1002/esp.2155>
- Huang HP, Yang KC and Lai, SW. (2007) Impact force of debris flow on filter dam. *Momentum* 9(2): 03218.
- Huang Y, Jin XY, Ji JJ (2022) Effects of barrier stiffness on debris flow dynamic impact—I: Laboratory flume test. *Water* 14(2): 177. <https://doi.org/10.3390/w14020177>
- Huang Y, Zhang B (2022) Challenges and perspectives in designing engineering structures against debris-flow disaster. *Eur J Environ Civ En* 26(10): 4476-4497. <https://doi.org/10.1080/19648189.2020.1854126>
- Hungr O, Morgan GC, Kellerhals R (1984) Quantitative analysis of debris torrent hazards for design of remedial measures. *Can Geotech J* 21(4): 663-677. <https://doi.org/10.1139/t84-073>
- Iverson RM (1997) The physics of debris flows. *Rev Geophys* 35(3): 245-296. <https://doi.org/10.1029/97RG00426>
- Kennedy RP (1976) A review of procedures for the analysis and design of concrete structures to resist missile impact effects. *Nucl Eng Des* 37(2): 183-203. [https://doi.org/10.1016/0029-5493\(76\)90015-7](https://doi.org/10.1016/0029-5493(76)90015-7)
- Kwan JS, Sze EH, Lam C (2019) Finite element analysis for rockfall and debris flow mitigation works. *Can Geotech J* 56(9): 1225-1250. <https://doi.org/10.1139/cgj-2017-0628>
- Liu D, You Y, Liu J, et al. (2019) Spatial-temporal distribution of debris flow impact pressure on rigid barrier. *J Mt Sci* 16(4): 793-805. <https://doi.org/10.1007/s11629-018-5316-4>
- Lu Y, Ju N, Zhang W, et al. (2019) Correction calculation of large stone impact force of debris flow grille dam. *Sci Technol Eng* 19(24): 76-81. (In Chinese)
- Luo G, Zhao, YJ, Shen WG, et al. (2022) An analytical method for the impact force of a cubic rock boulder colliding onto a rigid barrier. *Nat Hazards* 112(1): 603-618. <https://doi.org/10.1007/s11069-021-05196-5>
- Majeed ZZA, Lam NTK, Lam C, et al. (2019) Contact force generated by impact of boulder on concrete surface. *Int J Impact Eng* 132: 103324. <https://doi.org/10.1016/j.ijimpeng.2019.103324>
- Mao YM, Guo XL, Zhao Y. (2010) Experimental study of hammer impact identification on a steel cantilever beam. *Exp Tech* 34: 82-85. <https://doi.org/10.1111/j.1747-1567.2009.00530.x>
- Marchelli M, De Biagi V (2019) Dynamic effects induced by the impact of debris flows on protection barriers. *Int J Prot Struct* 10(1): 116-131. <https://doi.org/10.1177/2041419618798378>
- Mizuyama T (1979) Computational method and some considerations on impulsive force of debris flow acting on sabo dams. *J Jpn Soc Eros Control Eng* 112: 40-43.
- Ng CWW, Su Y, Choi CE, et al. (2018) Comparison of cushioning mechanisms between cellular glass and gabions subjected to successive boulder impacts. *J Geotech Geoenviron Eng* 144(9), 04018058. [https://doi.org/10.1061/\(ASCE\)GT.1943-5606.0001922](https://doi.org/10.1061/(ASCE)GT.1943-5606.0001922)
- Paczkowski K, Riggs HR, Naito CJ, et al. (2012) A one-dimensional model for impact forces resulting from high mass, low velocity debris. *Struct Eng Mech* 42(6): 831-847. <https://doi.org/10.12989/sem.2012.42.6.831>
- Sayed A, Attia WA (2012) Finite elements analysis techniques of vessel collision with cable-stayed bridge. *Life Sci* 9(2): 1179-1190.
- Shen W, Zhao T, Zhao J, et al. (2018) Quantifying the impact of dry debris flow against a rigid barrier by DEM analyses. *Eng Geol* 241: 86-96. <https://doi.org/10.1016/j.enggeo.2018.05.011>
- Si GW, Chen XQ, Chen JG, et al. (2022) The impact force of large boulders with irregular shape in flash flood and debris flow. *KSCE J Civ Eng* 26(10):4276-4289. <https://doi.org/10.1007/s12205-022-0680-6>
- Song D, Choi CE, Ng CWW, et al. (2019) Load-attenuation mechanisms of flexible barrier subjected to bouldery debris flow impact. *Landslides* 16(12): 2321-2334. <https://doi.org/10.1007/s10346-019-01243-2>
- Stolle J, Derschum C, Goseberg N, et al. (2018) Debris impact under extreme hydrodynamic conditions part 2: Impact force responses for non-rigid debris collisions. *Coast Eng* 141: 107-118. <https://doi.org/10.1016/j.coastaleng.2018.09.004>
- Tang JB, Hu KH (2018) A debris-flow impact pressure model combining material characteristics and flow dynamic parameters. *J Mt Sci* 15(12): 2721-2729. <https://doi.org/10.1007/s11629-018-5114-z>
- Vagnon F (2020) Design of active debris flow mitigation measures: A comprehensive analysis of existing impact models. *Landslides* 17(2): 313-333. <https://doi.org/10.1007/s10346-019-01278-5>
- Wang QC, Chen J, Wang H, et al. (2016) Impact force of boulders conveyed in debris flows on bridge piers and collision protection measures. *Int J Geohazards Environ* 2(2): 72-81. <https://doi.org/10.15273/ijge.2016.02.008>
- Wang Z, Liu D, You Y, et al. (2023) Characteristics of debris flow impact on a double-row slit dam. *J Mt Sci* 20(2): 415-428. <https://doi.org/10.1007/s11629-022-7462-y>
- Yamaguchi I (1985) Erosion control engineering. Tokyo: Society of Erosion Control Engineering.
- Yong ACY, Lam NTK, et al. (2020) Cantilevered RC wall subjected to combined static and impact actions. *Int J Impact Eng* 143: 103596. <https://doi.org/10.1016/j.ijimpeng.2020.103596>
- Zeng C, Cui P, Su Z, et al. (2015) Failure modes of reinforced concrete columns of buildings under debris flow impact. *Landslides* 12(3): 561-571. <https://doi.org/10.1007/s10346-014-0490-0>
- Zhang SC (1993) A comprehensive approach to the observation and prevention of debris flows in China. *Nat Hazards* 7(1): 1-23. <https://doi.org/10.1007/BF00595676>
- Zhang SJ, Chen J (2017) An experimental study: Integration device of fiber bragg grating and reinforced concrete beam for measuring debris flow impact force. *J Mt Sci* 14(8): 1526-1536. <https://doi.org/10.1007/s11629-016-4166-1>
- Zhang X, Wen ZP, Chen WS, et al. (2019a) Dynamic analysis of coupled train-track-bridge system subjected to debris flow impact. *Adv Struct Eng* 22(4): 919-934. <https://doi.org/10.1177/1369433218785643>
- Zhang SJ, Xu CX, Chen J, et al. (2019b) An experimental evaluation of impact force on a fiber Bragg grating-based device for debris flow warning. *Landslides* 16(1): 65-73. <https://doi.org/10.1007/s10346-018-1083-0>
- Zhang Z, He SM, Liu W, et al. (2019c) Source characteristics and dynamics of the October 2018 Baige landslide revealed by broadband seismograms. *Landslides* 16: 777-785. <https://doi.org/10.1007/s10346-019-01145-3>
- Zhang Y, Wei FQ, Wang Q (2007) Experimental research of reinforced concrete buildings struck by debris flow in mountain areas of western China. *Wuhan Univ J Nat Sci* 12(4): 645-650. <https://doi.org/10.1007/s11859-006-0339-z>
- Zhou BF (1991) Guidelines for debris flow control (1st ed.). Science Press. (In Chinese)
- Zhou XW, Zhang WC, Gao YS, et al. (2020) A Study of the cumulative impact forces of stainless-steel reinforced concrete pier. *Int J Steel Struct* 20(1): 13-22. <https://doi.org/10.1007/s13296-019-00266-8>